ESA Contract Report

SMOS ESL contract 4000130567/20/I-BG

Contract Report to the European Space Agency

Annual SMOS brightness temperature monitoring report - 2022/23

Authors: Kirsti Salonen, Pete Weston and Patricia de Rosnay
Contract officer: Raffaele Crapolicchio

November 2023

Series: ECMWF - ESA Contract Report

A full list of ECMWF Publications can be found on our web site under:

http://www.ecmwf.int/publications/

European Centre for Medium Range Weather Forecasts
Shinfield Park, Reading, RG2 9AX, England

Abbreviations

BUFR ..... Binary Universal Form for the Representation of meteorological data
CMEM ..... Community Microwave Emissivity Modelling platform
ECMWF ..... European Centre for Medium-range Weather Forecasts
ESA ..... European Space Agency
IFS ..... Integrated Forecast System
NRT..... Near Real Time
NWP..... Numerical Weather Prediction
RFI..... Radio Frequency Interference
SMAP ..... Soil Moisture Active Passive
SMOS ..... Soil Moisture and Ocean Salinity
Tb ..... Brightness Temperature

1. Introduction

This document provides an annual summary of the performance of the European Space Agency (ESA) Soil Moisture and Ocean Salinity (SMOS) brightness temperature (Tb) monitoring run routinely at the European Centre for Medium-range Weather Forecasts (ECMWF). The period covered is September 2022 to August 2023. Several different monitoring plots are presented, and notable features are discussed in detail. Also, potential improvements to the monitoring system are proposed.

2. Annual SMOS monitoring results

Routine operational monitoring of SMOS observations from the near real time BUFR (Binary Universal Form for the Representation of meteorological data) product is performed at ECMWF. The SMOS measured brightness temperatures are compared to short-term numerical weather prediction (NWP) forecasts transformed into brightness temperatures using the Community Microwave Emissivity Model (CMEM; de Rosnay et al. 2020). The CMEM outputs are simulated brightness temperatures in the Earth frame, and these are converted into the SMOS antenna frame using the geometric and Faraday rotation angles provided with each observation in the BUFR files. Differences between observations and their model counterparts are known as background departures and statistics of these background departures are accumulated and plotted routinely.

The samples used to produce the plots can be filtered by area, including global, Northern and Southern Hemispheres, as well as loose definitions of the continents: Europe (120°W-120°E, 35°N-77.5°N), Asia (0°W-120°W, 40°N-82.5°N), North America (120°E-0°E, 20°N-77.5°N), South America (120°E-0°E, 40°S-17.5°N) and Australia (0°E-120°W, 47.5°S-7.5°S). This section focuses on global statistics.

The plots are produced separately for data:

- Over sea or over land
- With different incidence angles: 30°, 40° or 50°
- With different polarisations: H (XX) or V (YY) at the SMOS antenna reference frame
- RFI unscreened/screened

A selection of different options for surface type, incidence angles and polarisations are presented, and the full set of plots for the RFI screened data are available via FTP at ftp://dpgswebserver-2.smos.eo.esa.int/SMOS_ESL2021/Task-5/Annual_Monitoring/2023/All_plots_2022_2023.zip).

A thorough introduction to the monitoring system can be found in Weston and de Rosnay (2022a) and examples of the plots produced can be seen at https://www.ecmwf.int/en/forecasts/quality-our-forecasts/monitoring/smos-monitoring, where also monitoring statistics for data without RFI screening are available. In this report the focus is on RFI screened data.

In this section each of the different types of plots produced as part of the SMOS monitoring system are presented and any notable features are highlighted to be investigated in more detail in the following sections.

2.1. Time series

In the time series figures, statistics are plotted as lines against time on the x-axis for the full twelve-month period with statistics accumulated in 12-hour chunks. The statistics plotted are mean and standard deviation of background departures, the mean observed and background brightness temperatures and number of observations. These plots allow global trends and jumps in the statistics to be identified.

Figures 1 and 2 show that the background departure statistics over land are generally very stable over the year. The mean background departures mostly vary between ±5K for H polarisations and ±3K for V polarisations with only very occasional global mean values outside of this range. The standard deviation of background departures has slightly more day-to-day variability but generally stay close to a value of ~17K for H polarisations and ~14 – 15K for V polarisations. Overall, the statistics are very similar compared to the corresponding values from 2021/22 (Weston and de Rosnay, 2022b) indicating that SMOS is behaving in a stable way. The apparent slightly better performance of the V polarisations over the H polarisations could be due to an instrument effect but it could also be due to differing performance of the CMEM observation operator used to convert the model soil moisture to brightness temperature. It should be noted that the background departures presented here do not have a bias correction applied and the statistics are consistent with those found between 2010 and 2016 without bias correction in de Rosnay et. al. (2020).

Figure 3 shows that there is mostly less annual variability in the background departure statistics over sea than over land. The number of observations between September 2022 and June 2023 is much more stable over sea due to proportionally smaller areas of ocean covered by sea-ice than snow-covered land areas. There are few notable spikes in the departure statistics over sea, namely in the end of January 2023 continuing to the first half of February and in mid-April. These are both related to known RFI events and are discussed in more details in Section 3. Interestingly there is also a small but visible trend of increased standard deviation for the background departures between December 2022 and February 2023, this is also further investigated in Section 3.

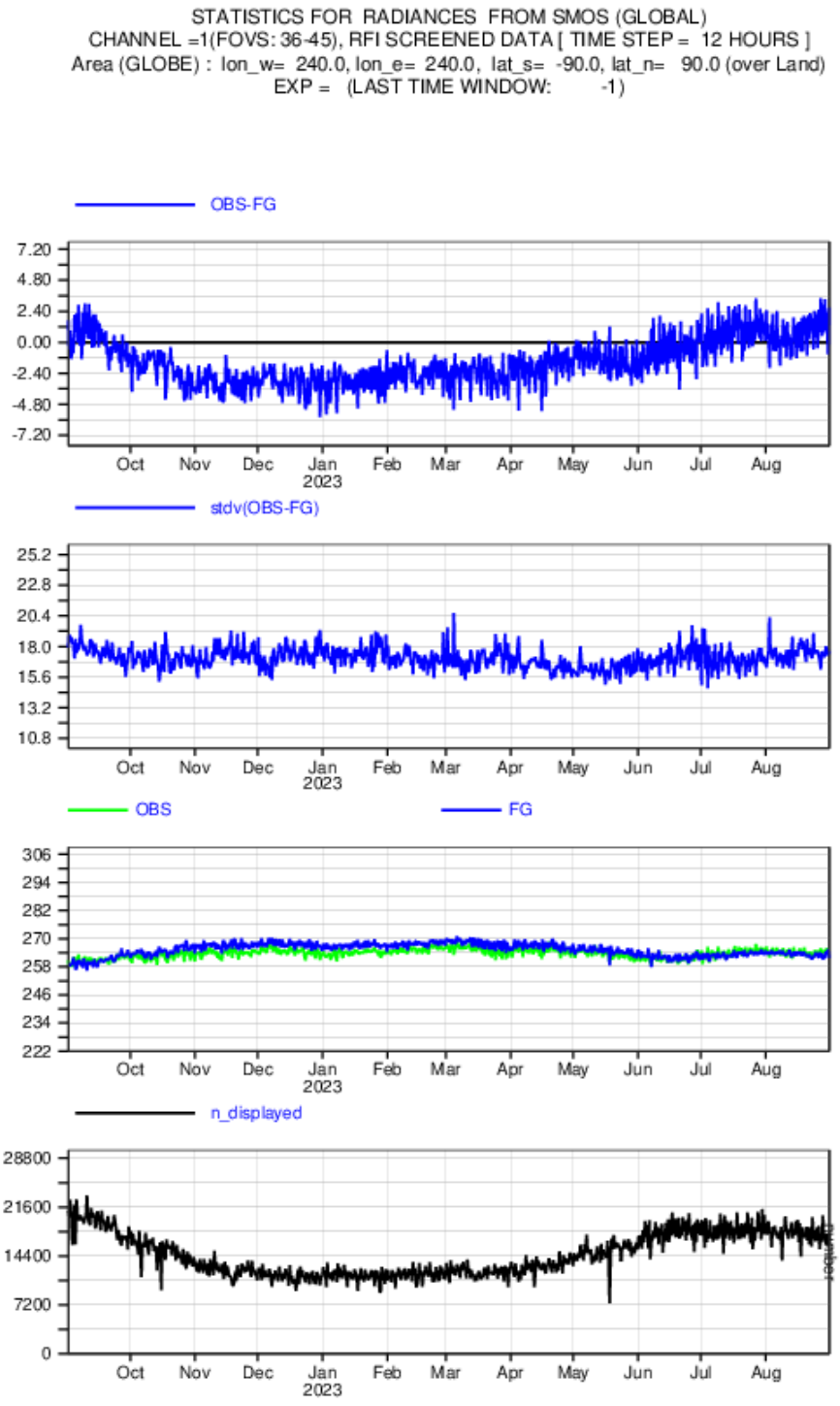

Figure 1: Time series of mean background departures (upper panel), standard deviation of background departures (2nd panel), mean observed and background values (3rd panel) and number of observations (lower panel). Statistics are accumulated into 12-hour bins for SMOS observations over land at 40° incidence angle, H polarisation and cover 1st September 2022 to 31st August 2023

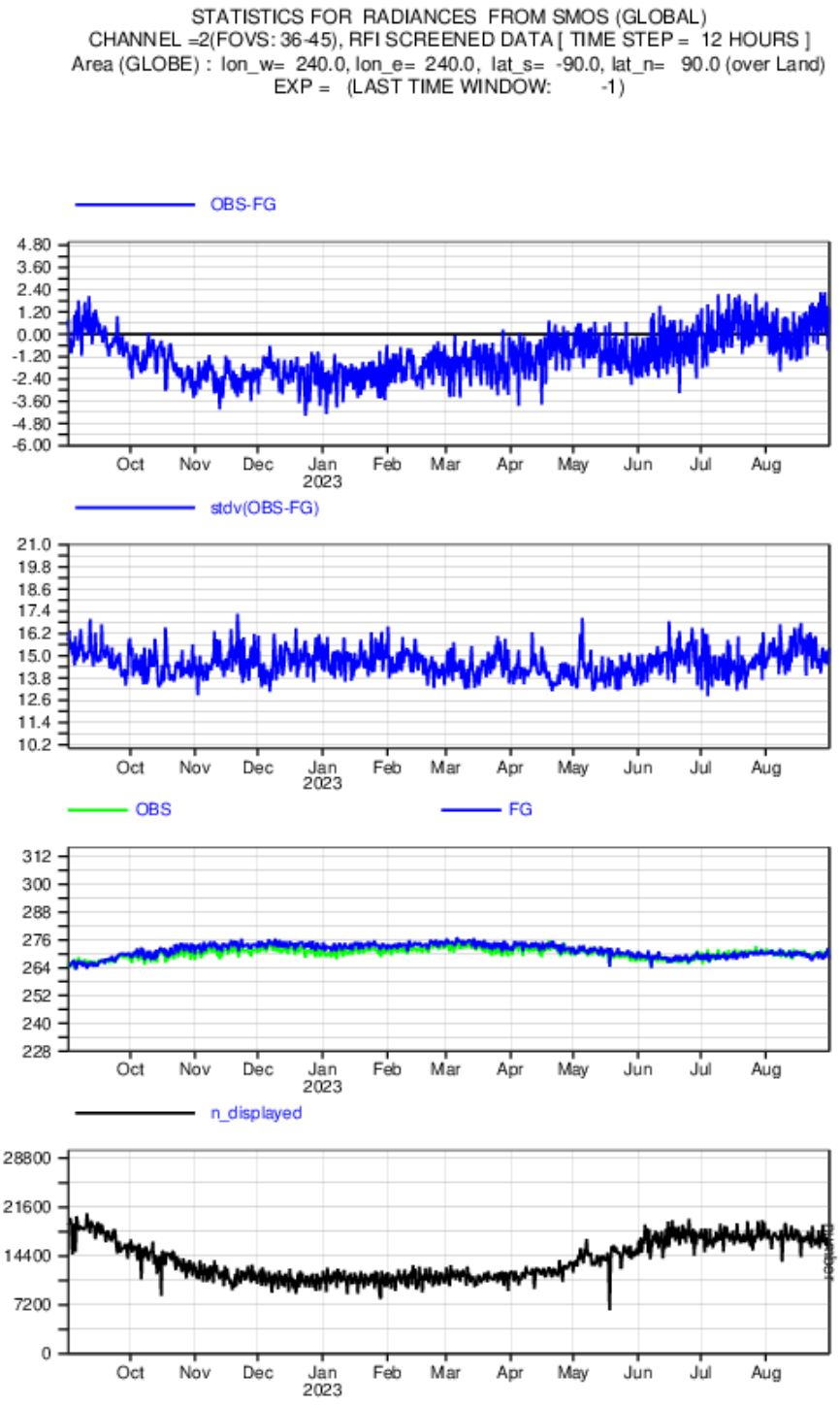

Figure 2: As figure 1 but for SMOS observations with V polarisation

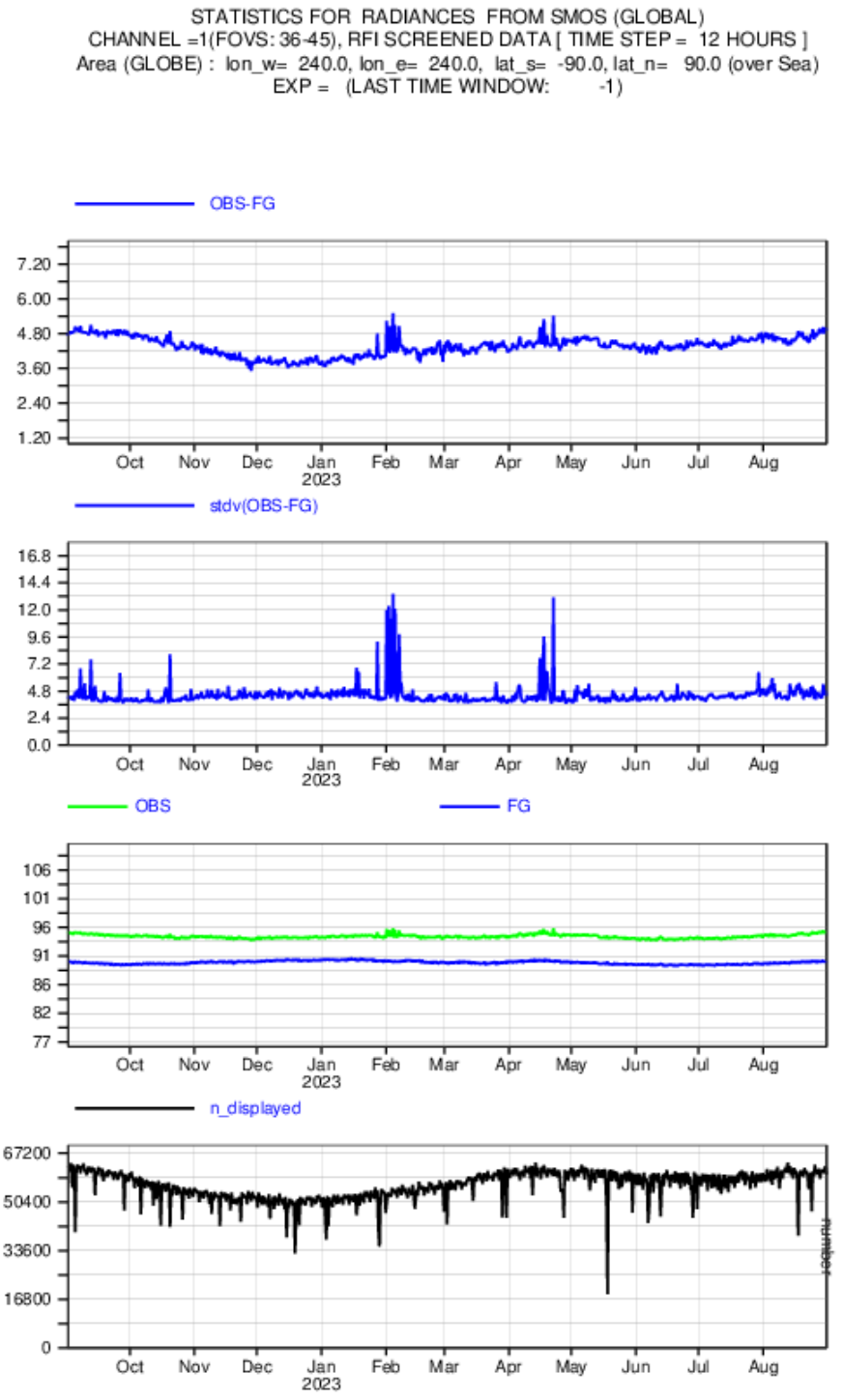

Figure 3: As figure 1 but statistics are accumulated for SMOS observations over sea at 40° incidence angle and H polarisation.

2.2. Hovmöller plots

Statistics presented in this section are plotted as a heat map (Hovmöller plot) with time on the x-axis and latitude on the y- axis for the twelve-month period with statistics accumulated in 2.5° latitude bins and 12-hour chunks. The statistics plotted are mean and standard deviation of background departure, mean and standard deviation of observed value and number of observations. These plots allow local trends and jumps in the statistics to be identified.

Figure 4 shows various seasonal patterns in the variability of the background departures over land for 30 incidence angle and V polarisation as an example of the monitoring results. There are areas of larger standard deviations of background departures at 10-30°N in September 2022 and June, July, August 2023 and 10-30°S in December 2022 to April 2023. These areas and times of year correspond to the wet season in the tropics and higher variability in model precipitation leading to higher variability in model soil moisture is the likely cause. There is also a large area of increased standard deviations of background departures between 60-80°N which corresponds to an area of positive bias in the background departures over Siberia. This is only visible in the Northern hemisphere (NH) summer because observations over these areas are screened out due to snow cover and frozen ground in NH winter. The feature can also be seen in the gridded maps in section 2.3. Generally, all incident angles and both H and V polarisations show signals of the same features.

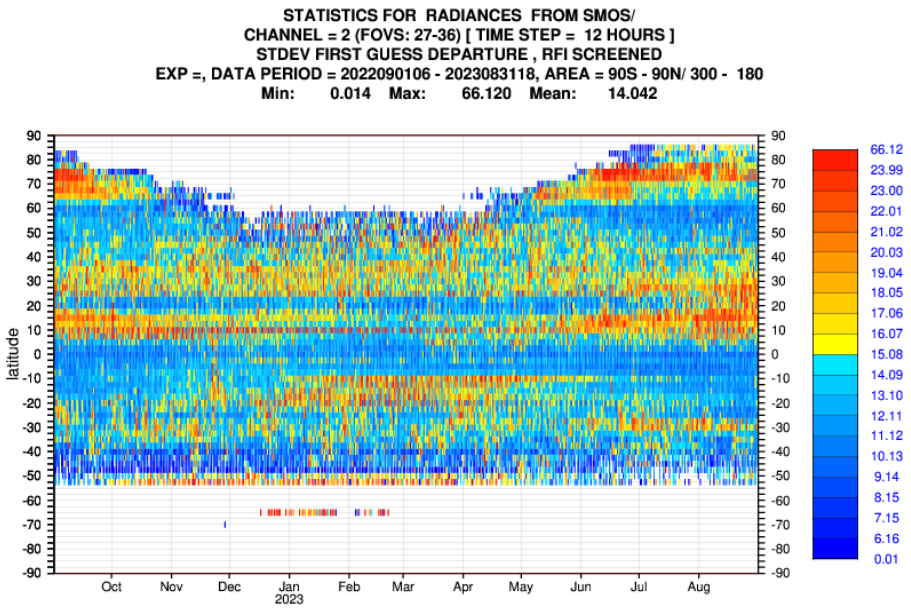

Figure 4: Hovmöller plot showing SMOS background departure standard deviation monitored over land at 30° incidence angle, V polarisation covering 1st September 2022 to 31st August 2023

Figure 5 shows the hovmöller plots for background departure standard deviation for incidence angles 30° (upper panel), 40° (middle panel) and 50° (lower panel) and H polarisation over sea. There is an interesting anomaly in the statistics occurring from November to February between 0 and 45°N. It is strongest for the incidence angle 30° and is gradually getting weaker for the higher incidence angles. The anomaly is present also for the statistics in V polarisation but slightly weaker in magnitude than for H polarisation (not shown).

Other notable features in Figure 5 include a strong increase in background departure statistics in late January – early February between between 30 and 60°N and in mid-April between 20 and 50°N. Both of these events are known to be related to new RFI sources. Further discussion of these events is presented in Section 3.

From December 2022 until the end of the monitoring period there is also strong increase in the departure statistics north of 70°N which is likely also RFI related. This is discussed more in the Section 2.3 where the statistics are shown on the gridded maps.

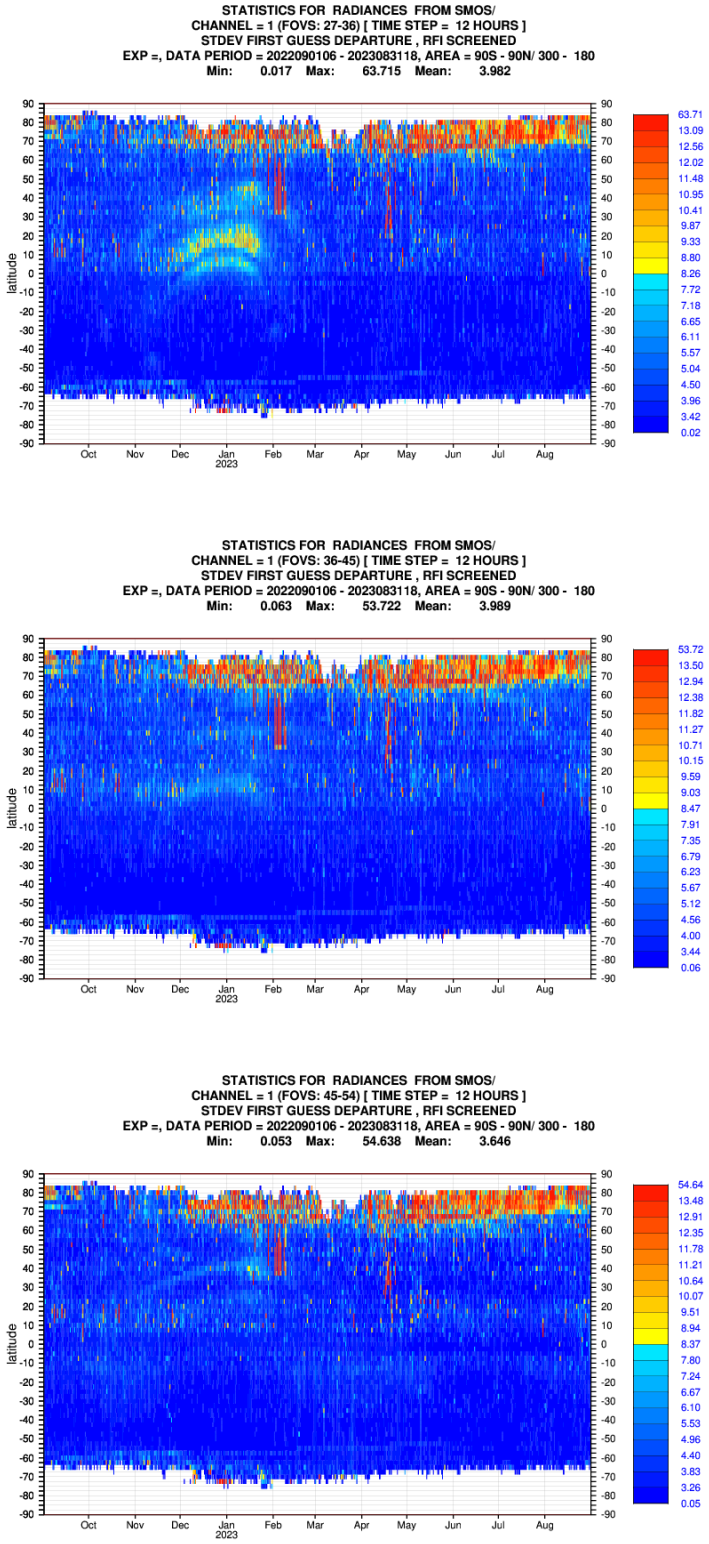

Figure 5: Hovmöller plots showing SMOS background departure standard deviation monitored over sea at H polarisation for 30° (upper panel), 40° (middle panel) and 50° (lower panel) incidence angle, respectively. The period covered is 1st September 2022 to 31st August 2023

2.3. Maps

Figure 6 shows the geographical distribution of biases in the SMOS background departures. Figures 1 and 2 indicate relatively small global mean background departures but figure 6 shows that there are areas with significantly large biases. Large positive biases are seen over Europe, Northern and Eastern Asia and South America, while large negative biases are evident over large parts of Africa, South-Western Asia, Australia and the far North of North America. The distribution of biases is very similar than reported for 2021/22 in Weston and de Rosnay (2022b).

Figure 7 shows that the largest variability in background departures remains over the Middle East, central and Eastern Asia, and to a lesser extent Europe. This is caused by RFI in those regions with the strength and location of RFI sources varying significantly throughout the year. The magnitude of these signals is comparable to 2021/22 monitoring results in Weston and de Rosnay (2022b). The improved v724 RFI screening in use since 2021 has significantly reduced the magnitudes of RFI signal in the statistics although Fig. 7 shows that the screening is still not perfect.

Figure 8 shows the background departure standard deviation over sea for incidence angle 50°, V polarisation. There are areas of increased background departures surrounding the coasts of Europe, in the Mediterranean Sea, North America and Asia as well as in the North Atlantic due to RFI contamination. Compared to 2021/22 (Weston and De Rosnay, 2022b) the RFI signals have significantly increased in the Arctic areas north of the Nordic countries and Russia. This is possibly related to the stronger military presence in the arctic area. Over the Northern and Southern polar regions there are slightly increased background departures due to a combination of smaller sample sizes due to sea-ice screening and slight sub-optimalities in the sea-ice screening during rapid melting and freezing events. Away from the RFI affected and polar regions there is very little variation in background departures due to lower Tb variations over ocean which are mostly caused by temperature variations. In addition, the observation operator CMEM treats the sea surfaces as flat surfaces like lake surfaces. Hence, there is currently no variation in simulated brightness temperature from waves or surface wind-speed as there will be in the observed brightness temperatures.

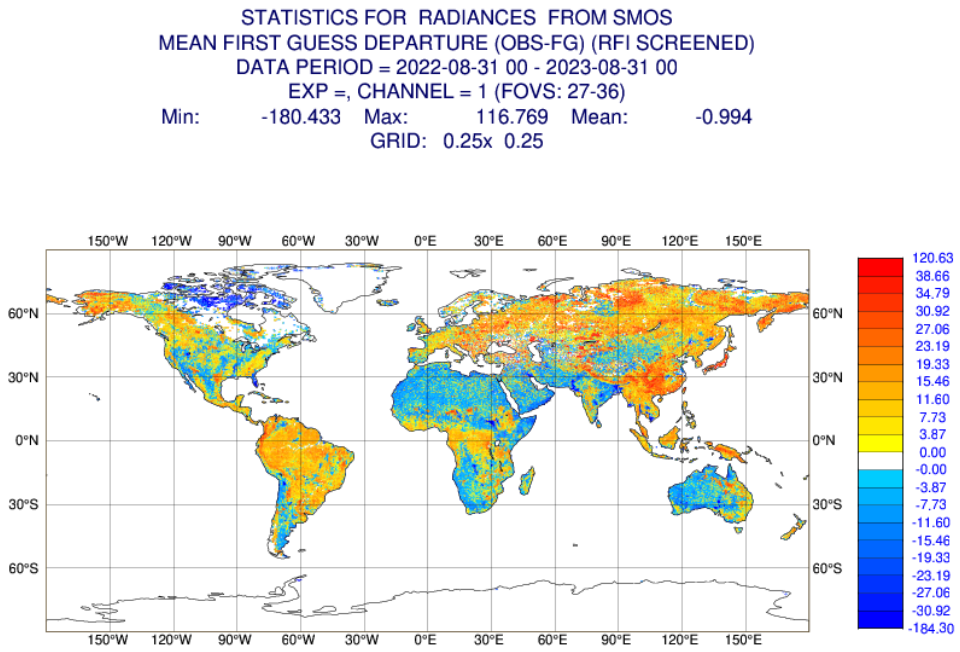

Figure 6: Gridded map plot showing the mean of SMOS background departures over land at 30° incidence angle, H polarisation covering 1st September 2022 to 31st August 2023

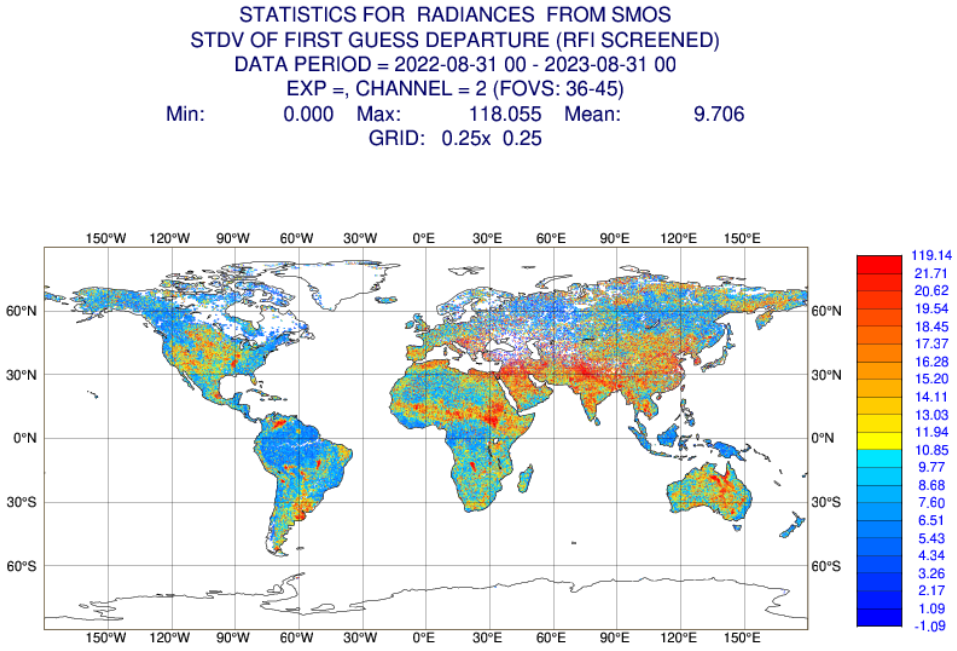

Figure 7: Gridded map plot showing the standard deviation of SMOS background departures over land at 40° incidence angle, V polarisation covering 1st September 2022 to 31st August 2023

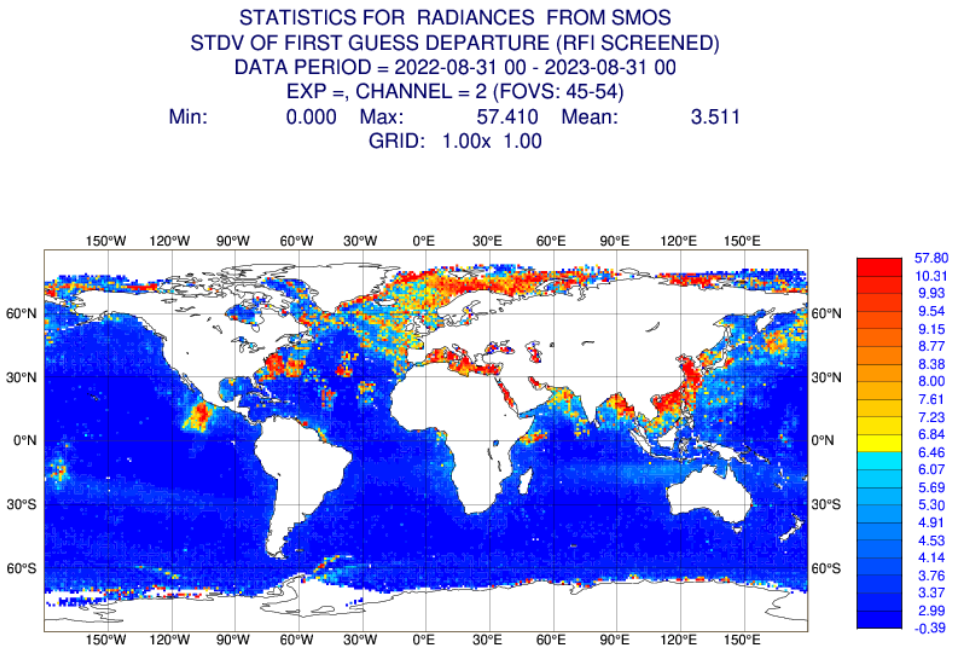

Figure 8: Gridded map plot showing the standard deviation of SMOS background departures over sea at 50° incidence angle, V polarisation covering 1st September 2022 to 31st August 2023

2.4. Scatter plots

In the scatter plots statistics are accumulated from 1st September 2022 to 31st August 2023 and plotted as a 2-dimensional histogram with incidence angle on the x-axis and background departure on the y-axis. These plots allow the distributions of background departures at different incidence angles to be analysed.

Figure 9 shows that the distribution of background departures is centred close to zero for all incidence angle bins. It also shows that the histograms are close to symmetric, which can be seen by looking at the number of observations in the background departure bins with a similar magnitude but opposite signs. The distributions of background departures are very similar than in 2021/22 (Weston and de Rosnay 2022b). The global mean background departures for each incidence angle bin are also close to zero although there are significant regional biases, see sections 2.3.

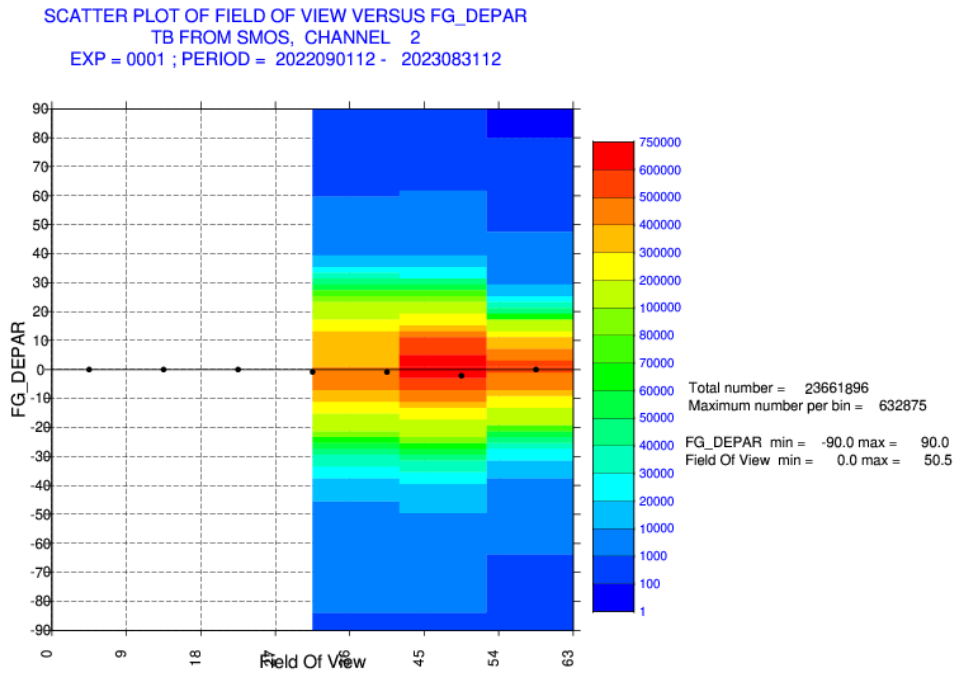

Figure 9: Scatter plot showing a 2D-histogram of SMOS background departures over land for different incidence angle bins, V polarization covering 1st September 2022 to 31st August 2023. The black dots represent the mean background departure for each incidence angle bin.

3. Notable features in 2022/23

This section describes notable features which are visible in the monitoring plots for September 2022 to August 2023.

3.1. Anomaly over sea December 2022 – January 2023

The Hovmöller plots discussed in Section 2.2 in Fig. 5 are showing an increase in the background departure standard deviations over sea surfaces from December 2022 to end of January 2023 between 0 and 45°N. The increase in the standard deviation is clear, especially for incidence angle 30° but the magnitude is notably smaller than seen for the known RFI events. To investigate this further, maps before, during and after the anomaly are compared.

Figure 10 shows monthly maps for the background departure standard deviation for the period October 2022 – March 2023, 30° incidence angle and H polarisation. In November a slight increase in the standard deviation is visible globally. In December further increase in the background departure statistics is very pronounced and limited to 0 – 45°N. The standard deviation of the departures is gradually getting stronger in magnitude within this latitude band in December and January, then decreasing in February and the statistics are back to normal levels, comparable to October 2022, in

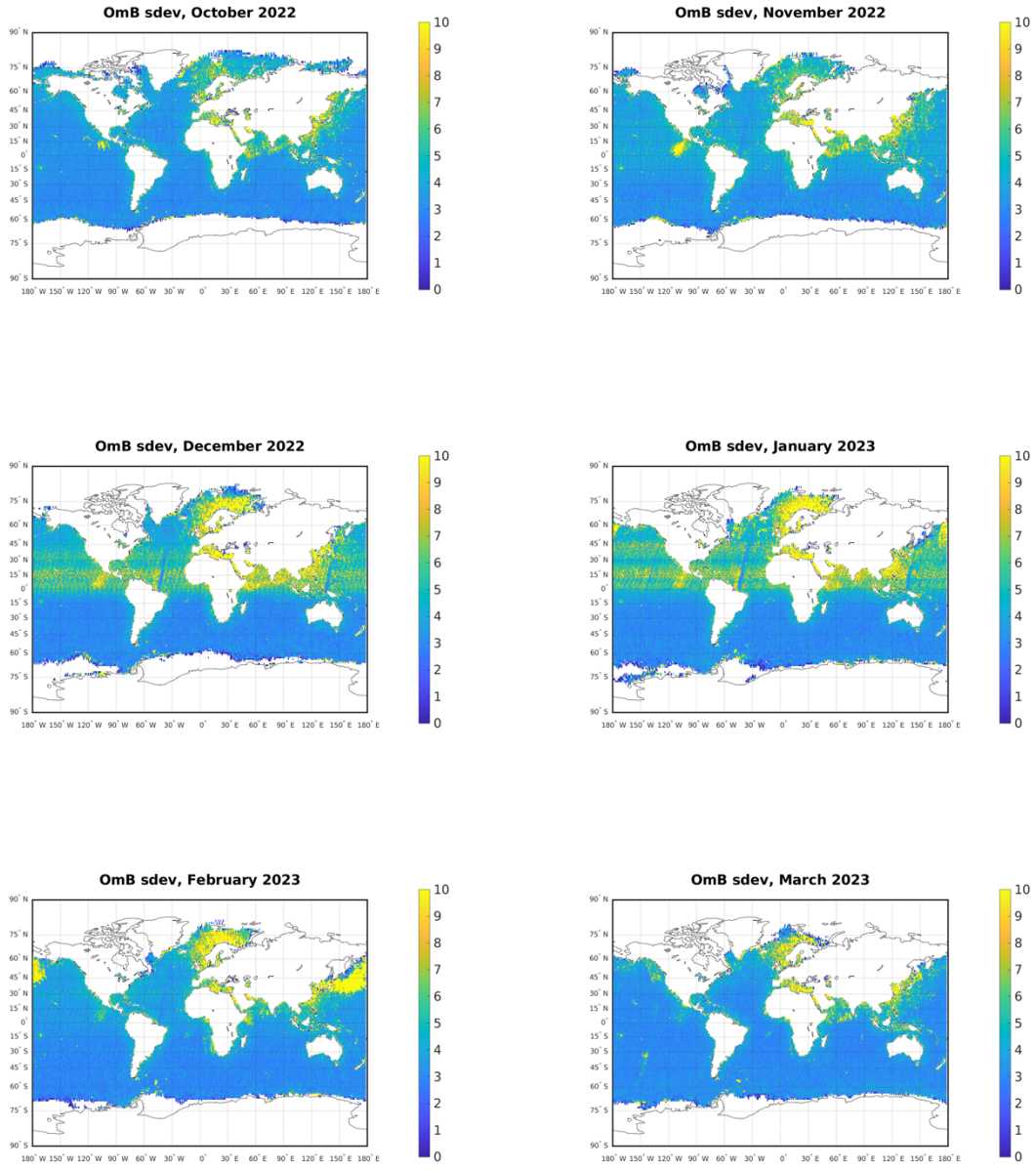

Figure 10: Monthly maps of the background departure standard deviation for incidence angle 30° and H polarization covering October 2022 – March 2023.

March 2023. The anomaly is affecting evenly the full 360° range of longitudes over sea but in latitude there are bands within the 0 – 45°N which are more strongly affected than others.

The SMOS brightness temperature monitoring includes both the alias-free and extended alias -free field of views (AF-FOV and EAF-FOV) (Weston and de Rosnay 2021). In Fig. 10 both are included in the statistics. To investigate if AF-FOV and EAF-FOV have different background departure characteristics during the anomaly, Fig. 11 shows the background departure standard deviation maps for AF-FOVs on the left panels and for EAF-FOVs on the right panels. Incident angles 30°, 40° and 50° are shown in the upper, middle and lower panels, respectively. The covered period is January 2023 when the anomaly is the strongest. The anomaly is visible for all incidence angles and both AF-FOV and EAF-FOVs. However, the increase in the background departure standard deviation is clearly stronger in magnitude for the EAF-FOV compared to the AF-FOVs. Note, that for incidence angle 50° there are very few observations in the EAF-FOV zone.

Figure 12 shows the standard deviation of observed values for AF-FOVs (left panel) and the EAF-FOVs (right panel) for incidence angle 30° and H polarisation for January 2023. The observations have increased variability over the regions where the anomaly is seen while the model background is very stable (not shown). The variability is stronger in the extended alias-free FOVs but is evident also for the alias-free FOVs. Figure 12 indicates that the anomaly is originating from the observations.

During the November 2022 – February 2023 period there is also an interesting pattern in the number of observations as illustrated in Fig. 13. In October 2022 the observation coverage is relatively even between the Northern and the Southern hemispheres. In November the number of observations south of 20°S has dropped, in December the drop is occurring south of 15°S and in January south of 10°S. In February 2023 there is also a drop in the number of observations over the northern hemisphere but in March the count has returned to be quite even on both hemispheres. The observation count in Fig. 13 is for the RFI screened observations that are monitored but similar behaviour is seen when RFI screening is deactivated (not shown).

Figure 14 shows the maps of number of observations (left panels) and the background departure standard deviation (right panels) separating the ascending passes (upper panels) and descending passes (lower panels) at H polarisation for 30° incidence angle over the month of January 2023. To complement, Fig. 15 shows Hovmöller plots of background departure standard deviation for ascending (left panel) and descending (right panel) passes covering the period of October 2022 – March 2023. It is clear that the increased background departure standard deviation as well as the changes in the number of observations are occurring for descending passes only, indicating that the anomaly is related to solar effect. During December 2022 – March 2023 the solar activity has been very strong, stronger than in the previous solar cycle in 2014. The strong solar activity can impact the accuracy of the faraday rotation due to higher uncertainty in the total electron content in the atmosphere.

In the ECMWF system, the quality control applied for SMOS brightness temperatures screens out observations where the solar reflection bit is set and these are not included to ODB files ingested by the model. The reduction in the number of observations seen in Fig. 13 and 14 is thus a consequence of the quality screening due to reflected sun. Despite the observations affected by solar effect are screened, the signal from the sun is spread on the entire snapshot and is seen as increased standard deviation of the observations and background departures. This is strong over the northern hemisphere where the sun

is in front of the antenna. On the contrary, in the ascending passes the sun is in the back of the antenna and its impact is attenuated by the antenna patter and the statistics are more homogeneous.

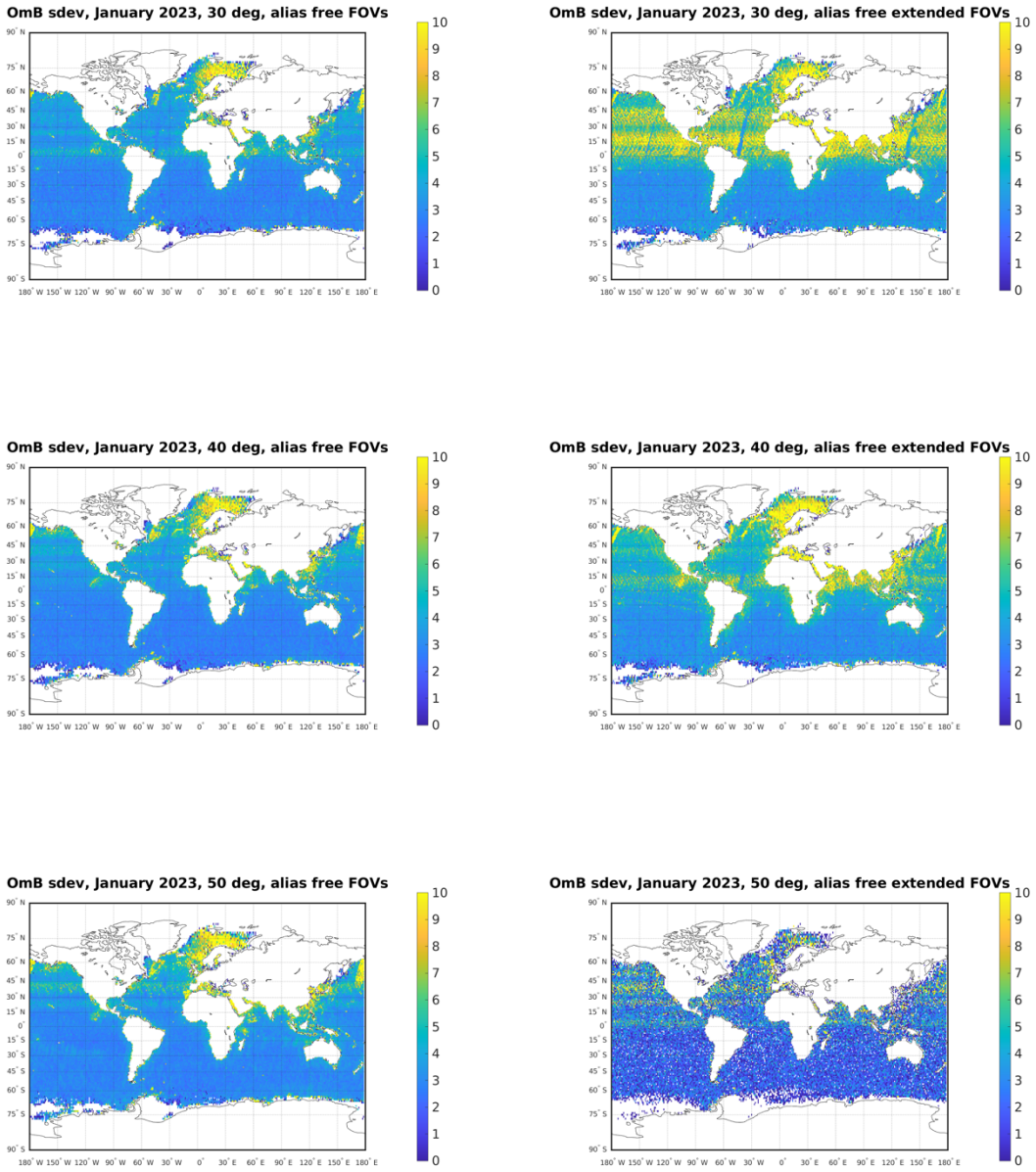

Figure 11: Maps of the background departure standard deviation for incidence angle 30° (upper panels), 40° (middle panels) and 50° (lower panels). The alias-free FOVs are shown on the left and extended alias-free FOVs on the right. The covered period is January 2023 and all statistics are for H polarization.

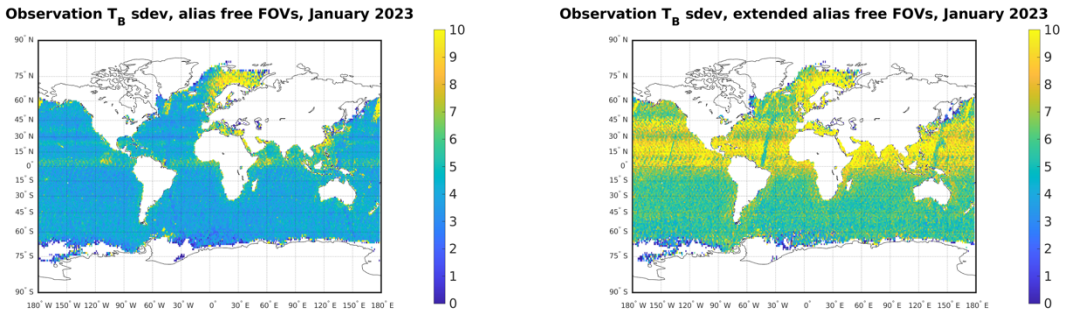

Figure 12: Maps of the observation standard deviation for incidence angle 30° and H polarisation. Left panel shows the alias-free FOVs and the right panel extended alias-free FOVs. The covered period is January 2023.

3.2. New RFI signal in Kamchatka peninsula late January – early February 2023

Figure 3 shows an increase in the magnitude of the mean and standard deviation of the background departures over sea during late January and early February and the Hovmöller plot in Figure 5 also gives a strong indication of increased background departure standard deviation over sea between 30°N and 60°N. A new strong RFI source was reported in the location 158.58E, 54.61N (located in Kamchatka peninsula) with brightness temperature around 150 000 K. It was suspected to be a radar type of signal. Although the most extreme values of SMOS brightness temperature (larger than 340 K or lower that 50 K) are discarded in the monitoring screening procedure, the quality control of lower values of affected brightness temperature relies on the SMOS product RFI flags. The RFI signal was first detected on 18th January 2023 and then on several days until 9th of February 2023. The source has not been detected since. Figure 16 shows maps of the background departure bias (left panels) and standard deviation (right panels) for 18th January – 9th February (upper panels) and for 10th – 28th February 2023 (lower panels). The increase in the background departure statistics seen in Figures 3 and 5 clearly originates from this source which has not been active since 10th February 2023.

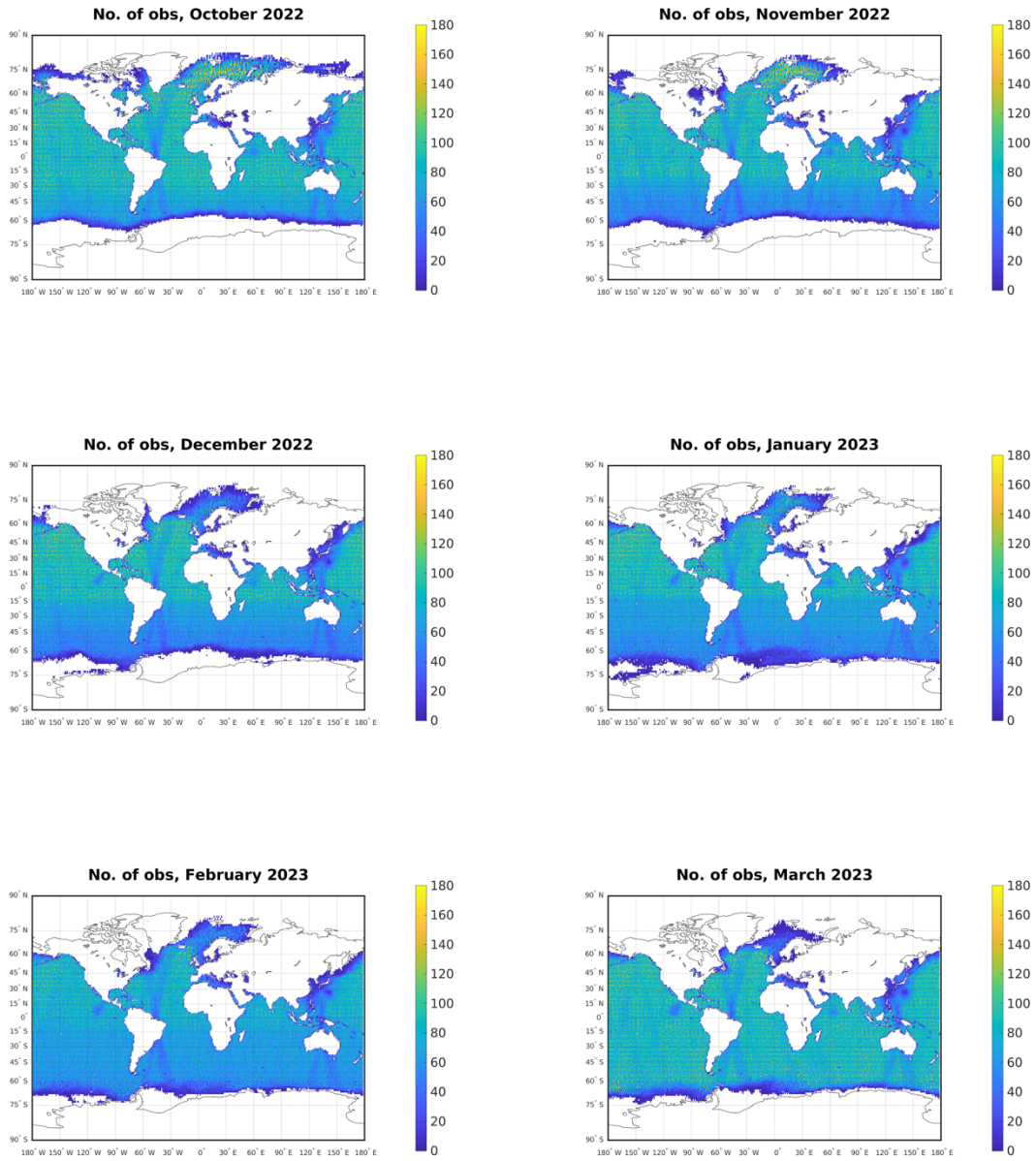

Figure 13: Monthly maps of number of observations accepted for monitoring for incidence angle 30° and H polarization covering October 2022 – March 2023.

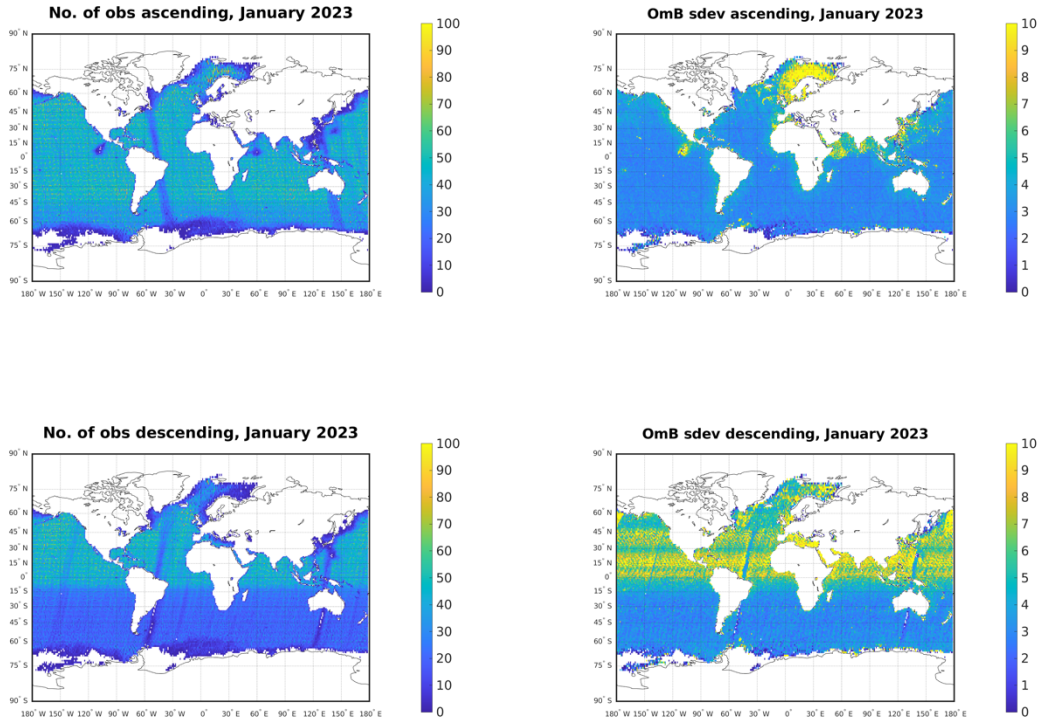

Figure 14: Maps for observation count (left panels) and background departure standard deviation (right panels) at H polarisation for 30° incidence angle for January 2023. The upper panels are for ascending passes and the lower panels are for the descending passes.

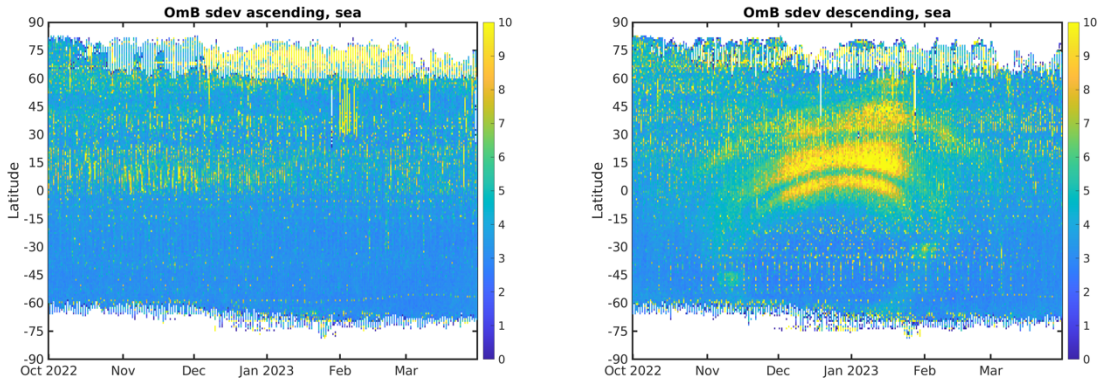

Figure 15: Hovmöller plots showing SMOS background departure standard deviation monitored over sea at H polarisation for 30° incidence angle for ascending passes (left panel) and descending passes (right panel), respectively. The period covered is 1st October 2022 to 31st March 2023.

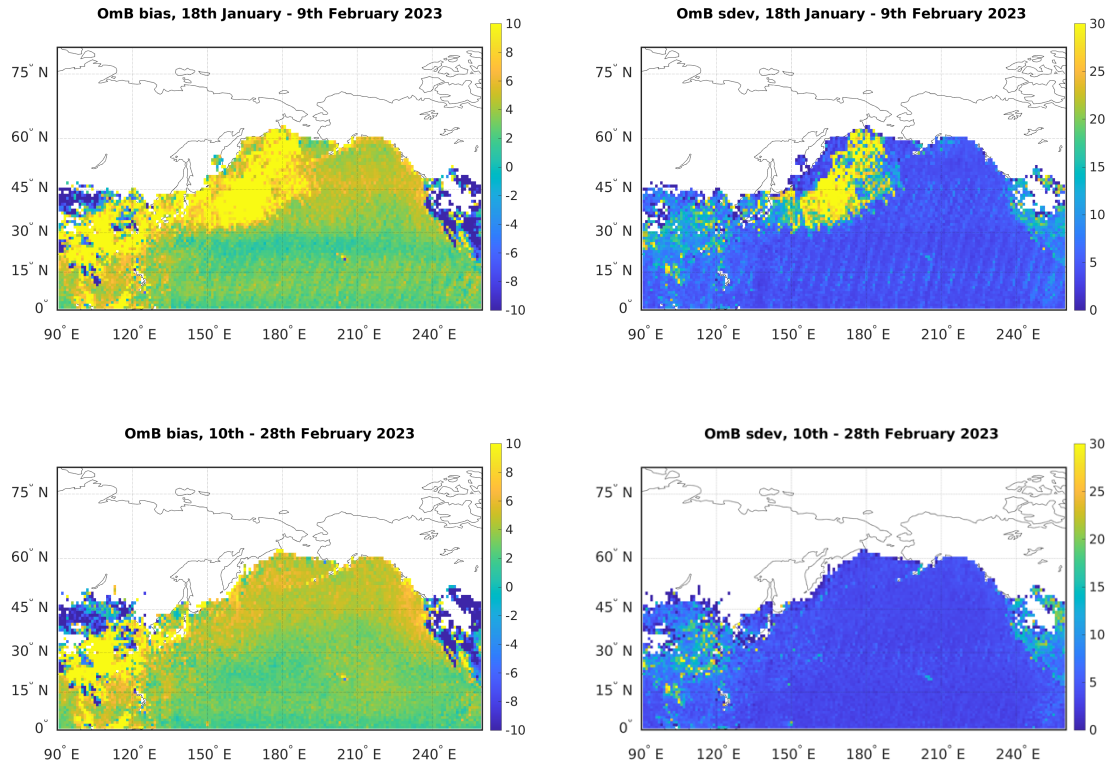

Figure 16: Maps for background departure (OmB) bias (left panels) and standard deviation (right panels) for 18th January – 9th February (upper panels) and for 10th – 28th February 2023 (lower panels).

3.3. New RFI signal in the North Atlantic 16th - 19th April 2023

Figure 3 indicates that there are increased background departure differences from 16th of April onwards for 4 days over sea. The increase in the departure statistics is evident also in Figure 5 which indicates that the signal originates from 20°N – 50°N. To investigate the feature further, figure 17 shows maps of the daily background departure standard deviations for 15th – 20th April 2023 for an area covering 30 - 120°W and 0 – 70°N. On 16th of April a new interfering source, possibly a ship, can be spotted in the North Atlantic. The RFI signal is getting stronger with moving location until it disappears on 20th April. The source has not re-appeared since, so no further action in the investigations has been taken.

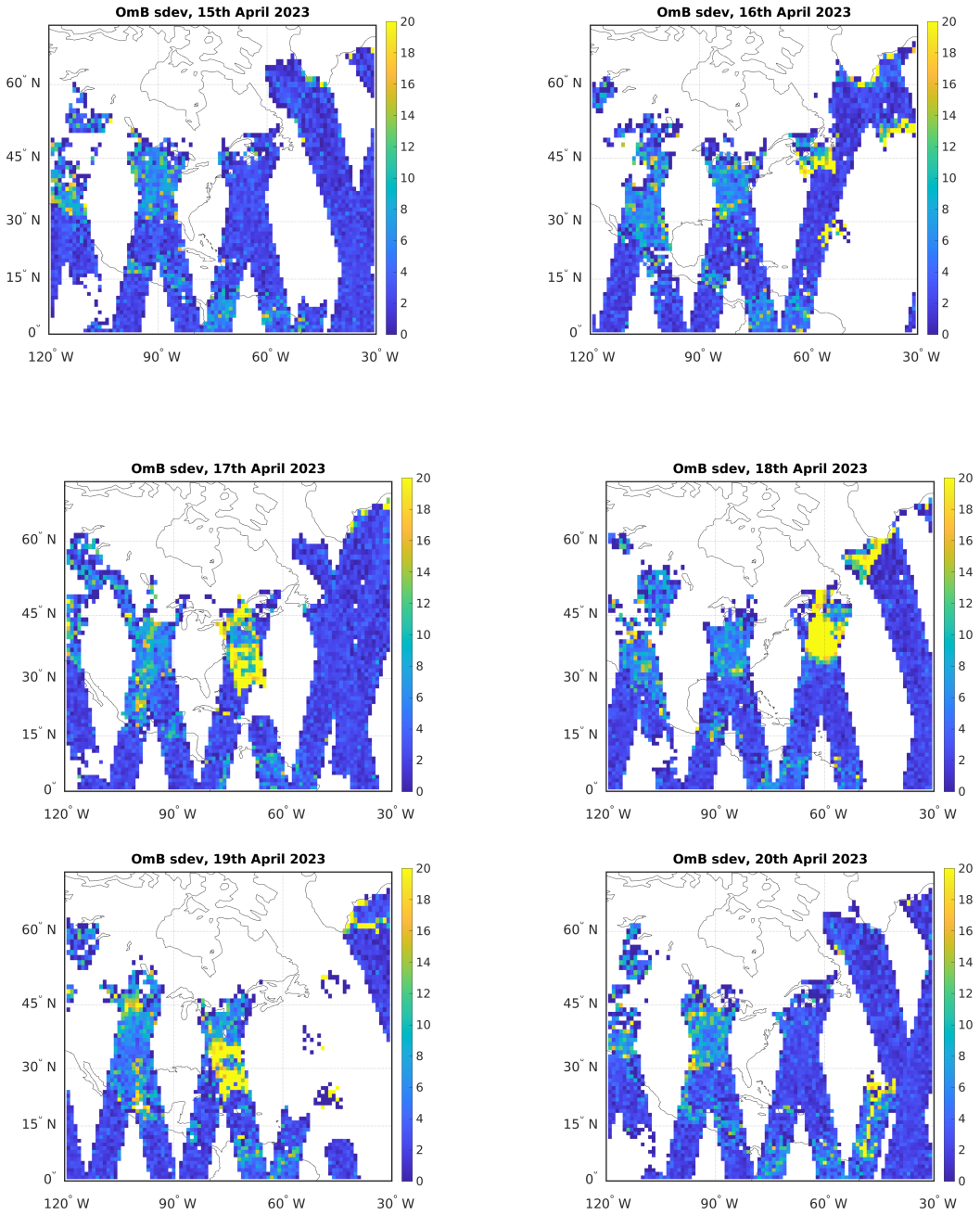

Figure 17: Maps of the daily background departure standard deviations for 15th – 20th April 2023 for an area covering 30 - 120°W and 0 – 70°N.

4. Comparisons to SMAP

Since 11th May 2021 the monitoring of the NASA Soil Moisture Active Passive (SMAP) instrument has also been part of the ECMWF operational system, using the same framework as the SMOS monitoring. SMAP was launched in 2015 and the instrument measures at L-band (1.41GHz) the same frequency as SMOS and therefore comparisons between the monitoring statistics for SMOS and SMAP are very relevant for unpicking observation and model issues in the background departures.

The comparisons presented in section 4.1 were made with data from November 2022 to August 2023 with the v724 SMOS L1 Tbs and most up-to-date SMAP Tbs in the operational system. SMAP had a major outage in August – October 2022 when the instrument was put in safe mode, meaning that no scientific data was measured. Thus, the full year cannot be considered in the comparison. The SMOS observations used in the comparison are limited to those with incidence angles between 39.5° and 40.5° which best match the 40° incidence angles of the SMAP observations. Also, the operational screening including the most up-to-date RFI screening is applied to the SMOS data. By contrast, SMAP has onboard RFI screening which is applied to the data before it arrives at ECMWF. CMEM with the same settings is used as the observation operator or both the SMOS and SMAP observations.

4.1. November 2022 to August 2023 comparison

Figure 18 shows that the standard deviation of background departures is slightly smaller for SMAP than for SMOS for V polarisation. For H polaristion the magnitudes are more similar (not shown). The SMAP mean background departures are more negatively biased with the magnitude of bias larger than for SMOS. Despite these small differences between SMOS and SMAP, the statistics are largely comparable and the results agree with comparisons made previously in Weston and de Rosnay (2022b).

Figure 19 shows that the gridded standard deviation values of background departures are significantly smaller for SMAP than they are for SMOS with the largest differences in Asia, the middle East and South-Eastern Europe, all areas where there are significant RFI sources. This indicates that the onboard screening for SMAP is still doing a better job than the v724 SMOS screening. In addition, over areas not affected by RFI, the SMAP standard deviation of background departures are also smaller than for SMOS albeit to a slightly lesser degree. This indicates that SMAP has lower instrument noise than SMOS which is expected because the SMOS instrument was designed to reduce the noise by averaging over different incidence angles. In this analysis only a small range of SMOS incidence angles are used so there is no reduction in noise from the use of multiple incidence angles.

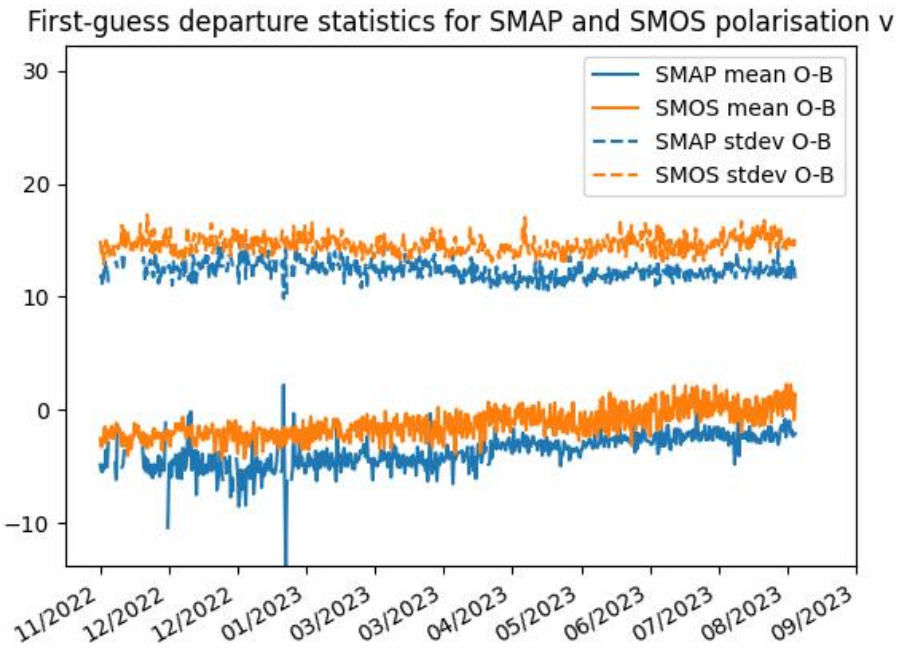

Figure 18: Time series of mean (solid lines) and standard deviation (dashed lines) of background departures for SMAP (blue) and SMOS (orange) for V polarisation between 1st November 2022 and 31st August 2023

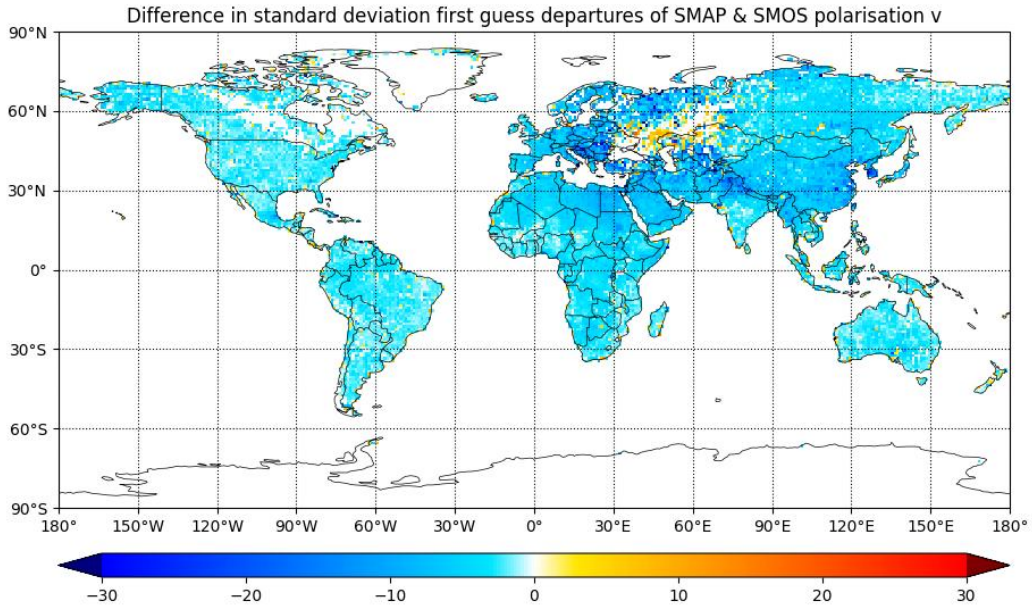

Figure 19: Difference in gridded standard deviation of background departures for V polarisation between SMAP and SMOS. Statistics are calculated between 1st November 2022 and 31st August 2023

5. Future enhancements to the monitoring system

5.1. Bias correction

An adaptive soil moisture bias correction scheme is under development for future implementation in the IFS in the next couple of years. It will complement the current CDF-matching approach which is used for soil moisture data assimilation into the simplified extended Kalman filter (SEKF). Applying this approach to the SMOS Tbs could be investigated in the future to improve on the results shown in section 3.3 and will be relevant for future assimilation experiments too.

5.2. Observation operator and model enhancements

As alluded to in section 2.1 , sub-optimalities in the observation operator are one of the potential sources of the residual biases in the SMOS background departures. As part of a new Horizon Europe project called CERISE (CopErnIcus Climate change Service Evolution), that started in January 2023, there will be work to enhance the observation operator for low frequency microwave observations in general (including at L-band frequencies) using machine learning approaches. This is expected to lead to improved performance leading to smaller biases in the SMOS background departures in the future. The timescale on this project is that the newly developed observation operator should be available in 2025.

Furthermore, developments in the ECMWF land surface model are ongoing to investigate the potential of a finer vertical discretization in the soil. This development is highly relevant to better represent the top-layers soil moisture dynamics, with expected potential improvements in model forward modelling capabilities. Machine learning approaches will be investigated to explore SMOS brightness temperature forward modelling using a multi-layer soil moisture approach.

References

de Rosnay, P., J. Muñoz-Sabater, C. Albergel, L. Isaksen, S. English, M. Drusch, J.-P. Wigneron: SMOS brightness temperature forward modelling and long term monitoring at ECMWF. Remote Sens. Environ., 237 (2020): 111424. https://doi.org/10.1016/j.rse.2019.111424

Liu, Q., Weng, F., and English, S.: An improved fast microwave water emissivity model, IEEE, T. Geosci. Remote, 49, 1238–1250, 2011.

Saunders, R., Hocking, J., Turner, E., Rayer, P., Rundle, D., Brunel, P., Vidot, J., Roquet, P., Matricardi, M., Geer, A., Bormann, N., and Lupu, C.: An update on the RTTOV fast radiative transfer model (currently at version 12), Geosci. Model Dev., 11, 2717–2737, https://doi.org/10.5194/gmd-11-2717-2018, 2018.

Weston, P., P. de Rosnay: Quality control plan for brightness temperature monitoring - 2022. ESA contract report. SMOS ESL contract 4000130567/20/I-BG, April 2022a

Weston, P., P. de Rosnay: Annual SMOS brightness temperature monitoring report - 2021/22. ESA contract report. SMOS ESL contract 4000130567/20/I-BG, December 2022b

Weston and de Rosnay; SMOS brightness temperature monitoring quality control review and enhancements, *13*(20), 4081, Remote Sensing, 2021 https://doi.org/10.3390/rs13204081